

# Development of transition edge sensor detectors optimized for single-photon spectroscopy in the optical and near-infrared

Peter C. Nagler<sup>a</sup>, S. Harvey Moseley<sup>a</sup>, Bernard J. Rauscher<sup>a</sup>, and John E. Sadleir<sup>a</sup>

<sup>a</sup>NASA/Goddard Space Flight Center, Greenbelt, MD USA

## ABSTRACT

The search for biosignatures in the atmospheres of exoplanets will be a key focus of future space telescopes that operate in the ultraviolet, visible, and near-infrared bands. Detection of biosignatures requires an instrument with moderate spectral resolving power ( $R \sim 100$ ) and a large bandwidth ( $\sim 400 \text{ nm} - \sim 1.8 \mu\text{m}$ ). Additionally, biosignature detection is a photon-starved science; instruments designed for these measurements would ideally combine high optical efficiency with quantum-limited photon detectors (i.e., detectors that exhibit zero dark current). In this work, we report on our efforts to develop energy resolving transition edge sensor (TES)-based detectors designed for biosignature detection. TESs operated as microcalorimeters are compelling detectors for this application. Unlike semiconductor detectors, TESs eliminate the need for dispersive optics and are truly single photon detectors – fundamental TES noise yields uncertainty in the energies of detected photons, not in the number of detected photons. We introduce TESs designed for this application and discuss the path toward realizing a TES-based dispersionless spectrometer optimized for biosignature detection.

**Keywords:** biosignature detection, exoplanets, transition edge sensor, integral field spectroscopy

## 1. INTRODUCTION

The search for life on other worlds holds pride of place in NASA’s 30-year strategic vision for astrophysics.<sup>1,2</sup> Already, concepts exist for a Large Ultraviolet-Optical-Infrared (*LUVOIR*) space telescope equipped with a coronagraph and a starshade-based Habitable ExoPlanet Imaging Mission (*HabEx*).<sup>3</sup> For either concept, once a promising “exoEarth” candidate is found, spectroscopic biosignature characterization (Figure 1) will be used to seek evidence of life.

Unfortunately, even with 12 meters of aperture, biosignature characterization is extremely photon starved. For example, assuming a solar twin at 15 pc and an Earth-twin seen at quadrature, the count rate is only  $\sim 0.006 \text{ ph s}^{-1} \text{ pix}^{-1}$  at 760 nm in the focal plane of a dispersed coronagraph.<sup>6,7</sup> This feeble flux includes contributions from the exoEarth, Zodiacal and extra-Zodiacal light, and assumes a coronagraph background that is dominated by these astronomical sources. With a source arrival rate (excluding backgrounds) of only about one photon every 6 minutes per pixel in a dispersed focal plane, a noiseless detector – i.e., a nearly quantum-limited single photon detector – is highly desirable.

In this work, we discuss the use of a transition edge sensor (TES) for biosignature detection. TESs are especially attractive biosignature detector candidates. In contrast to semiconductor detectors, TESs have no read noise (in the conventional astronomy sense) and no dark current. TESs are energy resolving; they offer the tantalizing prospect of non-dispersive imaging spectroscopy at sufficient resolving powers for biosignature detection. A TES spectrograph does not require a dispersing spectrograph’s heavy and complex optics because each pixel directly measures an incident photon’s energy. In Section 2, we provide a brief review of semiconductor single photon detectors, and introduce low temperature detectors as an alternative. In Section 3, we discuss the unique potential of a TES as a biosignature detector, especially noting the recent advances in signal processing that will enable a TES to meet the requirements imposed by biosignature detection. We show results of calculations that apply results of non-linear signal processing to realistic LUVOIR-type devices and discuss how we will improve upon earlier TES work in the optical to meet LUVOIR-type requirements. Finally, in Section 4, we discuss ongoing work on the path toward achieving a biosignature detection-capable TES.

---

Further author information: Send correspondence to Peter C. Nagler  
E-mail: peter.c.nagler@nasa.gov, Telephone: 1-301-286-3206

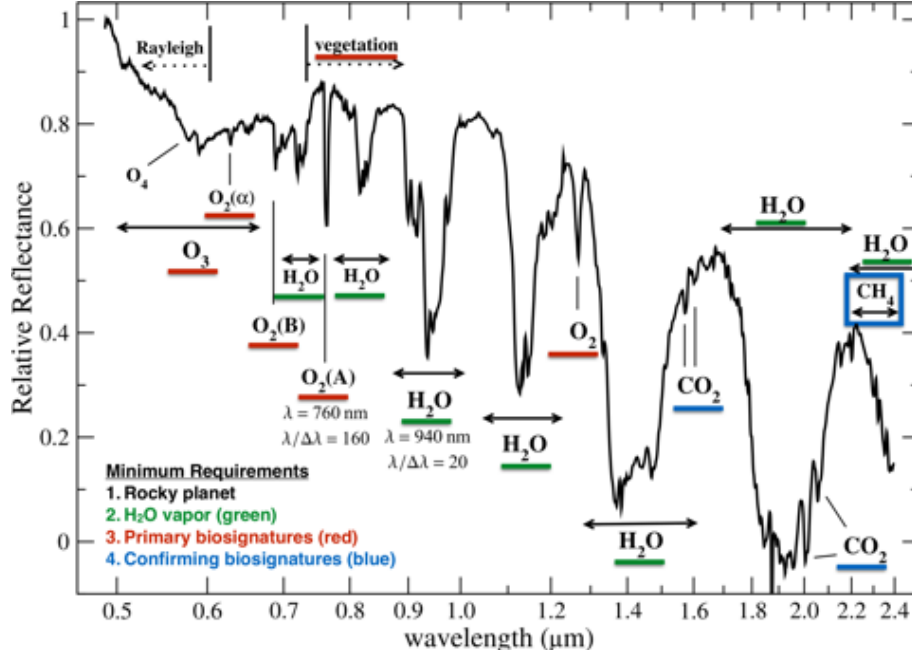


Figure 1. The Earth seen as an exoplanet. To make the spectrum, Turnbull *et al.*<sup>4</sup> observed the Earth, as reflected back by the night side of the moon. Biosignatures are atmospheric features that indicate potential life. Once a rocky planet is found, H<sub>2</sub>O is necessary for life as we know it. Biological processes can make O<sub>2</sub> and O<sub>3</sub>, although abiotic mechanisms (e.g., photo-dissociation of H<sub>2</sub>O) are possible. Confirming biosignatures<sup>5</sup> are needed to rule out false positives. H<sub>2</sub>O at  $\lambda = 940$  nm and O<sub>2</sub> at  $\lambda = 760$  nm are particularly important biosignatures. The 760 nm O<sub>2</sub> line sets the nominal requirement for resolving power,  $R = \lambda/\Delta\lambda > 100$ .

## 2. SINGLE PHOTON DETECTORS

A true single photon detector has zero uncertainty in the number of detected photons. Although several semiconductor-based “photon counting” detector technologies exist, of which  $e2v$ ’s electron multiplying CCD (EMCCD) is arguably the best known,<sup>8</sup> all semiconductor detectors add noise. This noise manifests itself as false positive or “dark” counts (where a photon is counted, but no photon actually arrived). As such, a semiconductor-based detector does not function as true single photon detector.

There are unavoidable practical reasons for this. All real semiconductors have imperfections, and some of these will manifest as electrically active defect states (charge “traps”) in the bandgap. For typical  $T \geq 80$  K visible and infrared (VISIR) detector operating temperatures, there will always be sufficient thermal energy in the semiconductor to promote some charges across the bandgap with the assistance of traps to appear as dark current. Even if one could make a perfectly defect-free crystal, once in space, proton irradiation would create defects, thereby undermining it for single photon detection.<sup>9</sup> Moreover, charge traps can manifest in other undesirable ways besides dark current; the charge transfer inefficiency degradation that plagues n-channel CCDs, including EMCCDs, is caused by trapping.

In contrast to detectors sensitive to single electron energetics and localized defect states, TES is a thermodynamic detector. The signal is a thermodynamic quantity (the temperature of the electron system in a solid) – the average of a very large system. A dark count event for the TES would occur if a noise record is mistaken for a thermal pulse. If we just recorded dark noise traces, and assuming typical sampling rates with a resolving power  $R \sim 4$ , a TES would give only one dark count – a false-positive in-band photon – per age of the universe. Another source of false positive occurs when two photons arrive at a pixel within a small time window. For the ExoEarth about 1 in every billion photons will fall within  $\pm 5$  ns of each other. But given that the *LUVOIR* bands considered only span a factor of 2 in energy, even these very rare events can be rejected with negligible impact on the absorption efficiency. Additionally, TESs are immune to local defects; they are composed of standard-coupling elemental BCS superconductors that have very large characteristic lengths ( $\sim 10$ ’s nm) that

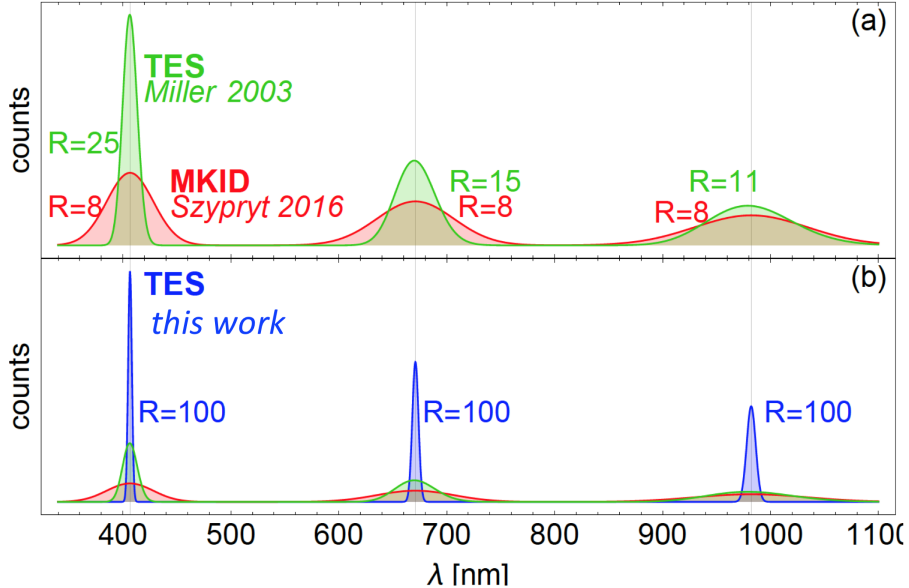


Figure 2. Built-in energy resolution line profiles of: (a) existing MKID and linear TES detector, (b) predicted response for a non-linear TES with resolving power  $R = 100$ . The line profiles show each respective detector’s response to the same number of photons at three wavelengths:  $\lambda = 406.6$  nm, 671 nm, and 982.1 nm. We show these photon energies because they represent published test data for the existing MKIDs and linear TESs.<sup>11,12</sup>

become significantly larger still very near the transition temperature  $T_c$ . For such superconductors, the energy gap and  $T_c$  are insensitive to nonmagnetic impurities and crystallographic defects (Anderson’s theorem).<sup>10</sup>

TESs have operated as single photon detectors in the optical and near-infrared (NIR) bands for decades,<sup>13,14</sup> often using W as the sensor material. Optical TES detectors developed at Stanford University achieved a resolving power  $E/\Delta E_{\text{FWHM}} \simeq 20$  during observations of Crab Nebulae.<sup>13</sup> More recently, optical TES detectors have been used for applications in quantum optics and quantum information science. These fields require a detector exhibiting extremely high detection efficiency, no dark counts, high count rates, and sufficient spectral resolution to resolve the number of incident monochromatic photons stemming from quantum optical processes. The TES energy resolution demonstrated by the Stanford group in 1998<sup>13</sup> is sufficient for these applications, so the most recent optical TES work has focused on achieving the highest system detection efficiency possible (with efficiencies now routinely in excess of ninety percent for fiber-coupled devices<sup>15</sup>) and in speeding up devices to accommodate high count rates. The latter is accomplished by raising the device’s operating temperature, trading energy resolution (already sufficiently high) for speed.<sup>16</sup> Figure 3 demonstrates the capability of a W TES to resolve 1550 nm (0.8 eV) photons<sup>17</sup> for the quantum optics applications. The energy resolution of this device is  $0.159 \pm 0.005$  eV. These efforts to increase speed and efficiency recently led to the first demonstrations of a loophole-free test of Bell’s inequality, a long-sought goal in experimental quantum physics.<sup>18</sup>

Although other low temperature detectors (LTDs) exist, including microwave kinetic inductance detectors (MKID), Superconducting Nanowire Single Photon Detectors (SNSPD), and Superconducting Tunnel Junction (STJ) arrays, TESs are uniquely promising in the context of biosignature detection. Compared to MKIDs, we believe that TESs uniquely promise to meet biosignature characterization’s  $R = \lambda/\Delta\lambda > 100$  spectral energy resolving requirement (see Figure 2). In contrast to SNSPDs, TESs are energy resolving.

Individual STJ detectors have achieved  $R \sim 7$ , but their use in astrophysics has been limited by the lack of an effective multiplexing system and the difficulty of optimizing STJs for efficient optical absorption over a wide wavelength range. In contrast, TES spectrometers can apply the full range of multiplexing systems developed for x-ray and CMB applications. For example, the LYNX x-ray mission under study for the 2020 decadal survey is developing a SQUID-based readout system for a focal plane consisting  $\sim 10^5$  TESs, larger than the nominal  $\sim 241 \times 241$  array needed for LUVOIR.

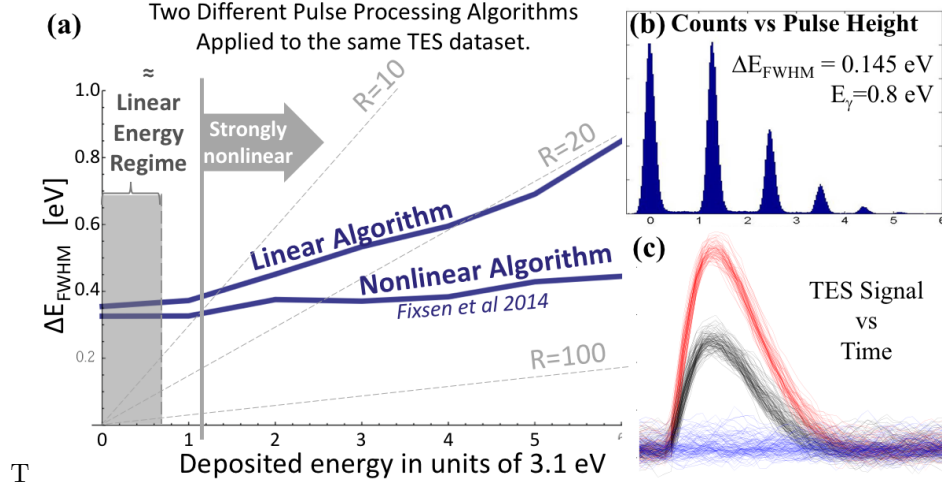


Figure 3. (a) Comparison of linear and non-linear pulse processing algorithms. The non-linear algorithm gives near-constant  $\Delta E_{FWHM}$  out to the largest photon energies measured. Gray dashed lines are contours of constant resolving power. Standard TES spectrometer design would be limited to photon energies in the shaded gray Linear Energy Regime. (b) Photon pulse height distribution measuring 1550 nm photons with  $\Delta E_{FWHM} = 0.145 \pm 0.005$  eV.<sup>17</sup> (c) Zero (blue), one (black), and two (red) photon pulses from a 785 nm laser measured by a W TES embedded in an optimized optical stack with  $T_c \sim 180$  mK.

### 3. THE TES AS A BIOSIGNATURE DETECTOR

In this section, we describe the path toward realizing a biosignature-detecting TES. We start with a review of the thermodynamics of a TES and the TES design considerations typically employed for a given spectroscopy application. Then we discuss a non-linear pulse processing algorithm recently developed at NASA/GSFC that greatly expands the parameter space over which a given device can operate. We present modeling results that show how a TES designed with the standard thermodynamic model can meet the requirements of a LUVOIR or HABEX-type mission by operating in the non-linear regime.

#### 3.1 Thermodynamic TES Model

The laws of thermodynamics, applied to any physical system with dissipation, require associated fluctuations in its state variables (noise). For a TES, the known thermodynamic fluctuations are associated with electrical resistance (Johnson noise in the TES resistance  $R_0$  and in the bias shunt resistor  $R_{sh}$ ) and thermal impedance (phonon noise or thermal fluctuation noise (TFN) across the thermal link  $G$ ). These noise sources set a fundamental thermodynamic limit on the achievable energy resolution  $\Delta E_{FWHM}$  of a TES. The expression for  $\Delta E_{FWHM}$ , the energy uncertainty due to thermodynamic noise, simplifies to a compact form<sup>19</sup> if we assume negligible amplifier noise, negligible shunt resistor Johnson noise, and large loop gain:

$$\Delta E_{FWHM} = 2\sqrt{2 \log 2} \sqrt{\frac{4k_B T_0^2 C \sqrt{n/2}}{\sqrt{1 - (T_b/T_0)^n}} \sqrt{\frac{1 + 2\beta}{\alpha^2}}}. \quad (1)$$

Here  $T_0$  and  $T_b$  are the temperature of the TES and bath respectively,  $n$  is a thermal exponent describing the power from through the thermal link  $G$  ( $n \simeq 5$  for electron-phonon conductance),  $C$  is the total heat capacity, and  $\alpha$  and  $\beta$  are both dimensionless parameters characterizing the sensitivity of the resistive transition to changes in temperature and current respectively, and  $\alpha$  and  $\beta$  are defined as the logarithmic derivative of the resistance with respect to temperature and current, respectively:  $\alpha = (T_0/R_0) \times (\delta R/\delta T)$  and  $\beta = (J_0/R_0) \times (\delta R/\delta J)$ . The expression simplifies further in the limit  $\beta \rightarrow 0$  and  $T_b \ll T_0$  to

$$\Delta E_{FWHM} = 2\sqrt{2 \log 2} \sqrt{4k_B T_0^2 \frac{C}{\alpha} \sqrt{n/2}}. \quad (2)$$

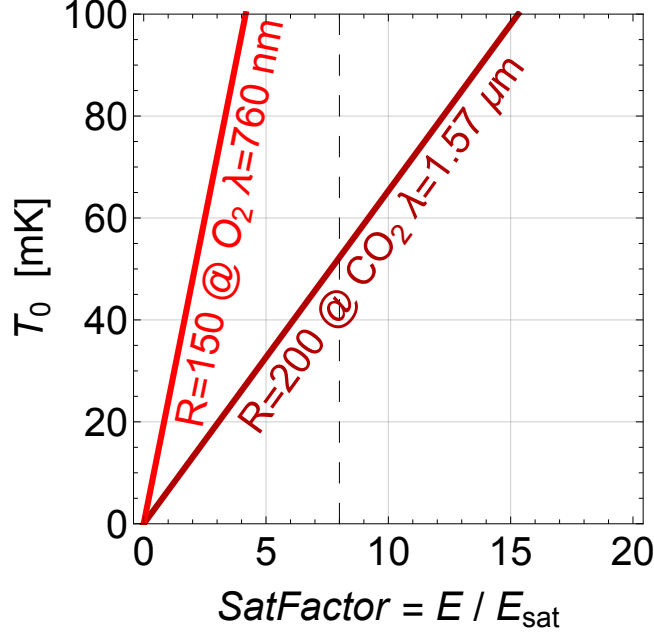


Figure 4. Illustration of the trade off between operating temperature  $T_0$  and nonlinearity ( $SatFactor$ ) for two important biosignature lines and resolving power  $R$  goals. The vertical dashed line is the most non-linear TES measurement, where  $\Delta E_{FWHM}$  is flat out to  $SatFactor = 8$ . Recognize that to satisfy  $R = 200$  at  $\lambda = 1.57 \mu\text{m}$  we can run the TES just as non-linear as Fixsen *et al.* at a temperature of 53 mK, or we can increase the  $SatFactor$  (more non-linear) and operate at a higher temperature. Until this point, TESs have been designed to operate in the linear regime, where  $SatFactor < 1$ . Compared to a linear TES, operating in the nonlinear regime enables significantly higher energy sensitivities for the same temperature. Beyond enabling a biosignature-detecting TES, this opens a new and exciting optimization space for TES applications across the electromagnetic spectrum.

From Equation 2, we see that we can reduce  $\Delta E_{FWHM}$  (thereby increasing sensitivity) by reducing the temperature, reducing the heat capacity, and increasing  $\alpha$ . Such changes increase the detector’s responsivity and for a linear device increase the pulse height (PH) of the current pulse  $|\delta J(t)|$  for the same photon energy. But the high-sensitivity part of the resistive transition exists only over a finite temperature range and the detector “saturates” for photon energies greater than  $E_{\text{sat}} = CT_0/\alpha$ . The finite temperature range of high sensitivity in the resistive transition and designing TESs to stay in the linear regime forces a tradeoff between the spectral range and the energy resolution.

To illustrate this tradeoff, we define the minimum and maximum photon energies in band of interest to be  $E_{\gamma\text{min}}$  and  $E_{\gamma\text{max}}$ , respectively. It is useful to define a unitless saturation factor  $SatFactor$ , defined as the ratio between the band’s maximum photon energy and the detector’s saturation energy:  $SatFactor = E_{\gamma\text{max}}/E_{\text{sat}}$ . The saturation factor measures how close to (or beyond) saturation the TES is for a particular application. The general approach for TES spectroscopy applications is to design the TES to operate within the linear regime over the entire photon energy band of interest. This means the devices are designed with the *requirement* that  $SatFactor < 1$ . Then a linear optimal filter can then be applied to each measured current pulse event to extract the photon’s energy. From Equation 2, this approach sets an upper limit on TES temperature  $T_0$  for a specific spectroscopy application. The standard design practice is to work with this  $T_0$  value (typically  $\alpha \sim 50$  to 1000 or more) and design the total heat capacity  $C$  such that the device saturates at the highest photon energy of interest. Applying this method to LUVOIR-like requirements, with  $0.69 \text{ eV} < E_{\gamma} < 3.1 \text{ eV}$  and  $E_{\gamma}/\Delta E_{FWHM} \geq 100$ , we find that the TES temperature  $T_0$  must be 5 mK or less for realistic device geometries and materials (Figure 4).

### 3.2 Non-linear TES operation

Many restrictions encountered in standard TES design can be lifted if a device can operate in the non-linear regime, where  $SatFactor > 1$ . There is significant evidence that this is a viable solution that greatly expands

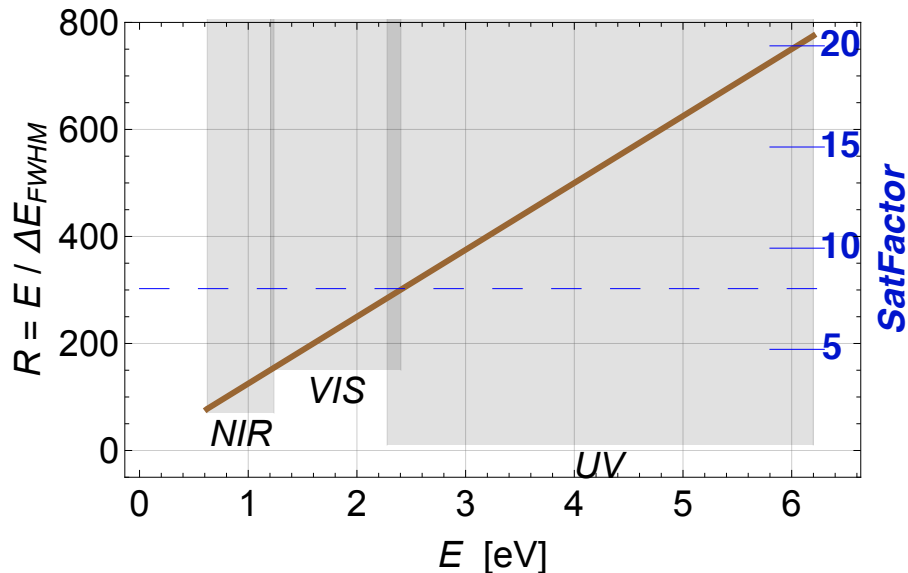


Figure 5. Left:  $R$  vs.  $E$  (brown) for a nonlinear TES with  $\Delta E_{\text{FWHM}} = 8$  meV. The shaded gray regions show each band considered for *LUVOIR* and its nominal  $R$  requirement (NIR:  $R \geq 70$ , VIS:  $R \geq 150$ , UV:  $R \geq 10$ ).<sup>7</sup> The device achieves  $R = 203$  at 760 nm ( $\text{O}_2$  line) and  $R = 98$  at 1570 nm ( $\text{CO}_2$  line). This TES operates at 70 mK and covers the entire NIR and VIS bands requiring no more non-linearity than already demonstrated by Fixsen *et al.*<sup>20</sup> With a larger *SatFactor*, we can either decrease  $\Delta E_{\text{FWHM}}$  or increase the TES operating temperature  $T_0$ .

the parameter space over which a TES can operate. Compared to linear operation, non-linear operation enables combinations of higher resolving powers, over broader bands, at higher operating temperatures.

Work by Fixsen *et al.*<sup>20</sup> (Figure 3) compares the standard linear optimal filter technique with the non-linear algorithm developed at NASA/GSFC for a dataset with non-linear TES pulse records at photon energies from 3 eV to 18 eV. The device under test was a W TES designed for quantum communications applications at  $\lambda = 1550$  nm (0.8 eV). The non-linear algorithm gives improved energy resolution at all energies measured. For the largest photon energy measured, the standard linear technique's  $\Delta E_{\text{FWHM}}$  increased by a factor of 2.4. The non-linear algorithm gives near-constant  $\Delta E_{\text{FWHM}}$  from the small signal value up to the largest energies measured at *SatFactor* = 8.

Busch *et al.*<sup>21</sup> achieved similar results. Data were on a MoAu TES taken using Al  $\text{K}\alpha$  (1.5 keV) and Mn  $\text{K}\alpha$  (5.9 keV) x-ray sources. The device was linear at 1.5 keV and non-linear at 5.9 keV. The resolving power achieved with the non-linear algorithm for 5.9 keV data was better than the resolving power achieved with a standard optimal filter for 1.5 keV data, giving  $R \sim 3200$  and  $R \sim 1800$ , respectively. Again we find the nonlinear algorithm improved the energy resolution out to the largest energies measured.

Assuming a realistic device designed with the thermodynamic TES model to meet required energy resolution in the linear regime, we modeled the relationship between operating temperature, resolving power, and *SatFactor*. The results are shown in Figures 4 and 5. Figure 4 shows the tradeoff between TES operating temperature and *SatFactor*. It illustrates that increasing the *SatFactor* means the TES can be operated at higher temperatures. The  $\text{CO}_2$  line at  $1.57 \mu\text{m}$  can be resolved at  $R = 200$  at a *SatFactor* that has already been demonstrated experimentally and at temperatures accessible to space-qualified cryostats. Achieving  $R = 150$  at the 760 nm  $\text{O}_2$  line requires even less saturation. Figure 5 demonstrates how a device operating at 70 mK can meet nominal *LUVOIR* requirements with the same non-linearity as the devices tested in Fixsen *et al.*<sup>20</sup>

#### 4. CONCLUSIONS

We show that the TES is a compelling candidate as a biosignature detector. It has no dark current, no read noise, and eliminates the need for a dispersive spectrometer. Already TESs have demonstrated better energy

resolving power than any other low temperature detector in the LUVUOIR band, despite little recent development for astrophysics applications. Advances in coupling light to a TES means they can now operate with near-unity efficiency, and a single broadband TES can satisfy biosignature detection requirements across the ultraviolet, optical, and near-infrared. Using the thermodynamic TES model (Section 3.1), we can design a device that meets biosignature detection requirements. For non-linear operation (Section 3.2), the device needs to meet the  $\Delta E_{\text{FWHM}}$  requirement at the lowest energy of the band where  $SatFactor < 1$ , and then not degrade as  $SatFactor$  increases. Up to the highest  $SatFactor$  measured to date, there is no observed degradation of  $\Delta E_{\text{FWHM}}$ . Compared to the best TES result in the optical by Miller *et al.*,<sup>12</sup> we will meet the  $\Delta E_{\text{FWHM}}$  requirements by: 1) reduce thermal fluctuation noise by reducing the operating temperature from 125 mK to 70 mK or lower; 2) reduce the heat capacity by reducing the TES volume or choosing a sensor material with fewer carriers; 3) reduce athermal phonon losses by building devices on a membrane or otherwise isolated substrate; 4) reduce hot quasiparticle losses by choosing a higher- $T_c$  lead material. We are currently in the process of building and testing devices that address each of these changes. Beyond adjusting each available parameter in the thermodynamic TES model, we will also explore device behavior under extreme saturation ( $SatFactor > 8$ ).

## REFERENCES

- [1] Kouveliotou, C., Agol, E., Batalha, N., Bean, J., Bentz, M., Cornish, N., Dressler, A., Figueroa-Feliciano, E., Gaudi, S., Guyon, O., Hartmann, D., Kalirai, J., Niemack, M., Ozel, F., Reynolds, C., Roberge, A., Straughn, K. S. A., Weinberg, D., and Zmuidzinas, J., “Enduring Quests-Daring Visions (NASA Astrophysics in the Next Three Decades),” *ArXiv e-prints* (Jan. 2014).
- [2] Dalcanton, J., Seager, S., Aigrain, S., Battel, S., Brandt, N., Conroy, C., Feinberg, L., Gezari, S., Guyon, O., Harris, W., Hirata, C., Mather, J., Postman, M., Redding, D., Schiminovich, D., Stahl, H. P., and Tumlinson, J., “From Cosmic Birth to Living Earths: The Future of UVOIR Space Astronomy,” *ArXiv e-prints* (July 2015).
- [3] Mennesson, B., Gaudi, S., Seager, S., Cahoy, K., Domagal-Goldman, S., Feinberg, L., Guyon, O., Kasdin, J., Marois, C., Mawet, D., Tamura, M., Mouillet, D., Prusti, T., Quirrenbach, A., Robinson, T., Rogers, L., Scowen, P., Somerville, R., Stapelfeldt, K., Stern, D., Still, M., Turnbull, M., Booth, J., Kiessling, A., Kuan, G., and Warfield, K., “The Habitable Exoplanet (HabEx) Imaging Mission: preliminary science drivers and technical requirements,” in [*Space Telescopes and Instrumentation 2016: Optical, Infrared, and Millimeter Wave*], *Proc. SPIE* **9904**, 99040L (July 2016).
- [4] Turnbull, M. C., Traub, W. A., Jucks, K. W., Woolf, N. J., Meyer, M. R., Gorlova, N., Skrutskie, M. F., and Wilson, J. C., “Spectrum of a Habitable World: Earthshine in the Near-Infrared,” *ApJ* **644**, 551–559 (June 2006).
- [5] Schwietzman, E. W., Meadows, V. S., Domagal-Goldman, S. D., Deming, D., Arney, G. N., Luger, R., Harman, C. E., Misra, A., and Barnes, R., “Identifying Planetary Biosignature Impostors: Spectral Features of CO and O<sub>4</sub> Resulting from Abiotic O<sub>2</sub>/O<sub>3</sub> Production,” *ApJ* **819**, L13 (Mar. 2016).
- [6] Stark, C. C., Roberge, A., Mandell, A., Clampin, M., Domagal-Goldman, S. D., McElwain, M. W., and Stapelfeldt, K. R., “Lower Limits on Aperture Size for an ExoEarth Detecting Coronagraphic Mission,” *ApJ* **808**, 149 (Aug. 2015).
- [7] Stark, C. C. Private communication (2017).
- [8] e2v. Online (2018).
- [9] Harding, L. K., Demers, R. T., Hoenk, M., Peddada, P., Nemati, B., Cherng, M., Michaels, D., Neat, L. S., Loc, A., Bush, N., Hall, D., Murray, N., Gow, J., Burgon, R., Holland, A., Reinheimer, A., Jorden, P. R., and Jordan, D., “Technology advancement of the CCD201-20 EMCCD for the WFIRST coronagraph instrument: sensor characterization and radiation damage,” *Journal of Astronomical Telescopes, Instruments, and Systems* **2**, 011007 (Jan. 2016).
- [10] Anderson, P., “Theory of dirty superconductors,” *Journal of Physics and Chemistry of Solids* **11**, 26–30 (Sept. 1959).
- [11] Szypryt, P., Mazin, B. A., Ulbricht, G., Bumble, B., Meeker, S. R., Bockstiegel, C., and Walter, A. B., “High quality factor platinum silicide microwave kinetic inductance detectors,” *Applied Physics Letters* **109**, 151102 (Oct. 2016).

- [12] Miller, A. J., Nam, S. W., Martinis, J. M., and Sergienko, A. V., “Demonstration of a low-noise near-infrared photon counter with multiphoton discrimination,” *Applied Physics Letters* **83**, 791 (July 2003).
- [13] Cabrera, B., Clarke, R. M., Colling, P., Miller, A. J., Nam, S., and Romani, R. W., “Detection of single infrared, optical, and ultraviolet photons using superconducting transition edge sensors,” *Applied Physics Letters* **73**, 735 (Aug. 1998).
- [14] Burney, J., Bay, T. J., Barral, J., Brink, P. L., Cabrera, B., Castle, J. P., Miller, A. J., Nam, S., Rosenberg, D., Romani, R. W., and Tomada, A., “Transition-edge sensor arrays for UV-optical-IR astrophysics,” *Nuclear Instruments and Methods in Physics Research A* **559**, 525–527 (Apr. 2006).
- [15] Lita, A. E., Miller, A. J., and Nam, S. W., “Counting near-infrared single-photons with 95% efficiency,” *Optics Express* **16**, 3032 (2008).
- [16] Lamas-Linares, A., Calkins, B., Tomlin, N. A., Gerrits, T., Lita, A. E., Beyer, J., Mirin, R. P., and Woo Nam, S., “Nanosecond-scale timing jitter for single photon detection in transition edge sensors,” *Applied Physics Letters* **102**, 231117 (June 2013).
- [17] Gerrits, T., Thomas-Peter, N., Gates, J. C., Lita, A. E., Metcalf, B. J., Calkins, B., Tomlin, N. A., Fox, A. E., Linares, A. L., Spring, J. B., Langford, N. K., Mirin, R. P., Smith, P. G. R., Walmsley, I. A., and Nam, S. W., “On-chip, photon-number-resolving, telecommunication-band detectors for scalable photonic information processing,” *Phys. Rev. A* **84**, 060301 (Dec. 2011).
- [18] Shalm, L. K., Meyer-Scott, E., Christensen, B. G., Bierhorst, P., Wayne, M. A., Stevens, M. J., Gerrits, T., Glancy, S., Hamel, D. R., Allman, M. S., Coakley, K. J., Dyer, S. D., Hodge, C., Lita, A. E., Verma, V. B., Lambrocco, C., Tortorici, E., Migdall, A. L., Zhang, Y., Kumor, D. R., Farr, W. H., Marsili, F., Shaw, M. D., Stern, J. A., Abellán, C., Amaya, W., Pruneri, V., Jennewein, T., Mitchell, M. W., Kwiatt, P. G., Bienfang, J. C., Mirin, R. P., Knill, E., and Nam, S. W., “Strong Loophole-Free Test of Local Realism\*,” *Physical Review Letters* **115**, 250402 (Dec. 2015).
- [19] Irwin, K. D. and Hilton, G. C., “Transition-edge sensors,” in [*Topics in Applied Physics: Cryogenic Particle Detection*], Enss, C., ed., Springer, Berlin (2005).
- [20] Fixsen, D. J., Moseley, S. H., Gerrits, T., Lita, A. E., and Nam, S. W., “Optimal Energy Measurement in Nonlinear Systems: An Application of Differential Geometry,” *Journal of Low Temperature Physics* **176**, 16–26 (July 2014).
- [21] Busch, S. E., Adams, J. S., Bandler, S. R., Chervenak, J. A., Eckart, M. E., Finkbeiner, F. M., Fixsen, D. J., Kelley, R. L., Kilbourne, C. A., Lee, S.-J., Moseley, S. H., Porst, J.-P., Porter, F. S., Sadleir, J. E., and Smith, S. J., “Progress Towards Improved Analysis of TES X-ray Data Using Principal Component Analysis,” *Journal of Low Temperature Physics* **184**, 382–388 (July 2016).